Theoretical Studies on Structures and Spectroscopic Properties of Bis-Cyclometalated Iridium Complexes

Tao Liu,[†] Bao-Hui Xia,[†] Xin Zhou,[†] Hong-Xing Zhang,*[,†] Qing-Jiang Pan,[‡] and Jin-Sheng Gao[‡]

State Key Laboratory of Theoretical and Computational Chemistry, Institute of Theoretical Chemistry, Jilin University, Changchun 130023, People's Republic of China, and College of Chemistry, Heilongjiang University, HaErBin 150080, People's Republic of China

Received July 13, 2006

The series of iridium(III) complexes $Ir(C^N)_2LX$ (C^N = bzq, LX = acac, **1**; C^N = thp, LX = acac, **2**; C^N = tpy, LX = acac, **3**; C^N = bzq, LX = dbm, **4**; acac = acetoylacetonate, bzq = benzoquinoline, tpy = 2-(4-tolyl)pyridine, thp = 2-(2′-thienyl)pyridine and dbm = dibenzoylmethanate) have been investigated theoretically to explore their electronic structures and spectroscopic properties. Their structures in the ground and excited states have been optimized at the B3LYP/LANL2DZ and CIS/LANL2DZ levels, respectively. The calculated bond lengths of Ir−N, Ir−C, and Ir−O in the ground state agree well with the corresponding experimental results. Upon excitation, the bond lengths of Ir−N and Ir−C lengthen by 0.03 Å and that of Ir−O shortens by 0.01 Å compared with those in the X^1A ground states. This is consistent with the variation trend of corresponding vibration mode in the ground and excited states. At the TD-DFT and PCM levels, **1**−**4** give rise to absorptions at 484, 462, 452, and 536 nm and phosphorescent emissions at 541, 589, 499, and 540 nm, respectively. The transitions of **1**−**3** are attributed to [d(Ir) + π(C^N)] → [π*(C^N)] charge transfer, whereas those of **4** are related to [d(Ir) + π(C^N)] → [π*(LX) + π*(C^N)]. It is shown that the emissions are significantly dominated by the metal participating in the frontier molecular orbitals and affected by the C^N ligands but are hardly perturbed by the LX ligands.

Introduction

Phosphorescent materials have attracted much attention, due to their potential application as highly efficient electroluminescent (EL) emitters in organic light emitting devices (OLEDs).[1] It is found that, in theory, OLEDs based on phosphorescence have higher internal quantum efficiency (75%) compared with those based on fluorescence (25%).[2] In principle, the phosphorescence originating from the triplet excited states is spin-forbidden but can be achieved through the spin−orbit coupling effect of the heavy metal. In this aspect, complexes containing d^6 metal ions such as ruthenium(II),[3] osmium(II),[4] rhenium(I),[5,6] rhodium(III),[7] and iridium(III)[8] have been extensively studied by various spectroscopic and electrochemical techniques. On the other hand, their long-lived triplet state emissions with high luminescent efficiencies increases the likelihood of either energy or electron transfer occurring before radiative or nonradiative relaxation; therefore, they have been applied as biological labeling reagents,[9] photocatalysts for CO_2 reduction,[10] and sensors.[11]

Usually, the Ru(II), Os(II), and Re(I) complexes exhibit lower energy absorptions (400−500 nm), which are predominantly assigned to dπ(M) → π*(ligand) charge transfer (MLCT) transitions. Their emissions have been ascribed to ^{3}MLCT transitions in both theoretical studies and experiments.[12−14] The analogue Ir(III) also has the same d^6 electronic configuration, but Ir(III) complexes have been less investigated, for these kinds of complexes are difficult to prepare. However, since it was reported that OLEDs prepared with $Ir(ppy)_3$ (ppy^- = 2-phe-

* To whom correspondence should be addressed. E-mail: Zhanghx@mail.jlu.edu.cn.

† Jilin University.

‡ Heilongjiang University.

(1) (a) Wand, Y.; Herron, N.; Grushin, V. V.; LeCloux, D. D.; Petrov, V. A. *Appl. Phys. Lett.* **2001**, *79*, 449. (b) Xin, H.; Li, F. Y.; Shi, M.; Bian, Z. Q.; Huang, H. C. *J. Am. Chem. Soc.* **2003**, *125*, 7166. (c) Tsuboyama, A.; Iwawaki, H.; Furugori, M.; Mukaide, T.; Kamatani, J.; Igawa, S.; Moriyama, T.; Miura, S.; Takiguchi, T.; Okada, S.; Hoshino, M.; Ueno, K. *J. Am. Chem. Soc.* **2003**, *125*, 12971.

(2) Adachi, C.; Baldo, M. A.; Forrest, S. R.; Thompson, M. E. *Appl. Phys. Lett.* **2000**, *77*, 904.

(3) (a) Smothers, W. K.; Wrighton, M. S. *J. Am. Chem. Soc.* **1983**, *105*, 1067. (b) Wang, Y. S.; Liu, S. X.; Pinto, M. R.; Dattelbaum, D. M.; Schoonover, J. R.; Schanze, K. S. *J. Phys. Chem. A* **2001**, *105*, 11118.

(4) Tung, Y. L.; Wu, P. C.; Liu, C. S.; Chi, Y.; Yu, J. K.; Hu, Y. H.; Chou, P. T.; Peng, S. M.; Lee, G. H.; Tao, Y.; Carty, A. J.; Shu, C. F.; Wu, F. I. *Organometallics* **2004**, *23*, 3745.

(5) Dominey, R. N.; Hauser, B.; Hubbard, J.; Dunham, J. *Inorg. Chem.* **1991**, *30*, 4754.

(6) Sacksteder, L.; Lee, M.; Demas, J. N.; DeGraff, B. A. *J. Am. Chem. Soc.* **1993**, *115*, 8230.

(7) Shinozaki, K.; Takahashi, N. *Inorg. Chem.* **1996**, *35*, 3917.

(8) Lamansky, S.; Djurovich, P.; Murphy, D.; Abdel-Razzaq, F.; Lee, H. E.; Adachi, C.; Burrows, P. E.; Forrest, S. R.; Thompson, M. E. *J. Am. Chem. Soc.* **2001**, *123*, 4304.

(9) (a) Lo, K. K. W.; Chung, C. K.; Lee, T. K. M.; Lui, L. H.; Tsang, K. H. K.; Zhu, N. Y. *Inorg. Chem.* **2003**, *42*, 6886. (b) Lo, K. K. W.; Ng, D. C. M.; Chung, C. K. *Organometallics* **2001**, *20*, 4999.

(10) (a) Silaware, N. D.; Goldman, A. S.; Ritter, R.; Tyler, D. R. *Inorg. Chem.* **1989**, *28*, 1231. (b) Belmore, K. A.; Vanderpool, R. A.; Tsai, J. C.; Khan, M. A.; Nicholas, K. M. *J. Am. Chem. Soc.* **1988**, *110*, 2004.

(11) Djurovich, P. I.; Thompson, M. E. *J. Am. Chem. Soc.* **2001**, *124*, 14828.

(12) Fang, Y.-Q.; Taylor, N. J.; Hanan, G. S.; Loiseau, F.; Passalacqua, R.; Campagna, S.; Nierengarten, H.; Dorsselaer, A. V. *J. Am. Chem. Soc.* **2002**, *124*, 7912.

(13) Yam, V. W.-W.; Wong, K. M.-C.; Chong, S. H.-F.; Lau, V. C.-Y.; Lam, S. C.-F.; Zhang, L. J.; Cheung, K.-K. *J. Organomet. Chem.* **2003**, *670*, 205.

(14) Ma, Y. G.; Zhang, H. Y.; Shen, J. C.; Che, C. M. *Synth. Met.* **1998**, *94*, 245.

10.1021/om0606338 CCC: $37.00
Publication on Web 11/30/2006

nylpyridine) have efficiencies greater than 80%, Ir(III) complexes have attracted much more attention.[8,15−19] Ir(III) has stronger spin−orbital coupling relative to Rh(II), resulting in intense phosphorescence at room temperature for the former complexes but measurable emission at low temperatures for the latter complexes. Furthermore, the phosphorescent lifetimes of the Ir complexes are longer ($\tau \approx 1-14\ \mu$s)[8,15,20] than those of other metal complexes (Ru(N^N^N)L,[12] 8−200 ns; Re(N^N)-(CO)$_3$(C≡CR),[13] 0.2 μs; Os(CN)$_2$(PH$_3$)Ph,[14] 0.62 μs). Thus, Ir-(III) complexes are good candidates for emitters in OLEDs. Recently, a series of Ir(III) complexes with cyclometalated (C^N) ligands (ppy = phenylpyridine, thp = 2-(2′-thienyl)-pyridine, tpy = 2-(4-tolyl)pyridine, bzq = benzoquinoline, etc.) and monoanionic, bidentate ligands LX (acac = acetoylacetonate, pico = picolinate, sal = *N*-methylsalicylimine, dbm = dibenzoylmethanate, etc.) have been synthesized by Thompson[8,15] and co-workers. The structures and absorption and emission spectra of the complexes were measured in 2-methyltetrahydrofuran media. In addition, these complexes as the phosphors were doped into the emissive layer of the OLEDs, giving a maximum optical output of 32 500 cd/m^2.

Although there have been many experimental studies on the photophysical and photochemical properties of luminescent Ir-(III) metal complexes,[21] corresponding theoretical reports on the complexes have been sparse. A deep insight into the luminescent mechanism of these kind of complexes is imperative and significant. Although Thompson[8] and Hay[16] et al. have investigated the luminescent properties of several Ir(III) complexes, they could not interpret the spectroscopic properties from an electronic structure point of view. Using the background given above, we began the present work, aimed at providing an in-depth theoretical understanding of the structures and spectroscopic properties of Ir(III) cyclometalated complexes. The revelation of the electronic structures and spectroscopic properties of the Ir(III) metal complexes should help us to design good phosphorescent materials. Herein, we performed theoretical calculations on Ir(bzq)$_2$(acac) (**1**), Ir(thp)$_2$(acac) (**2**), Ir(tpy)$_2$-(acac) (**3**), and Ir(bzq)$_2$(dbm) (**4**) in the ground and excited states using ab initio and density functional theory (DFT) methods. Furthermore, the effects of the peripheral ligands on the phosphorescence have been revealed so that the luminescence can be adjusted.

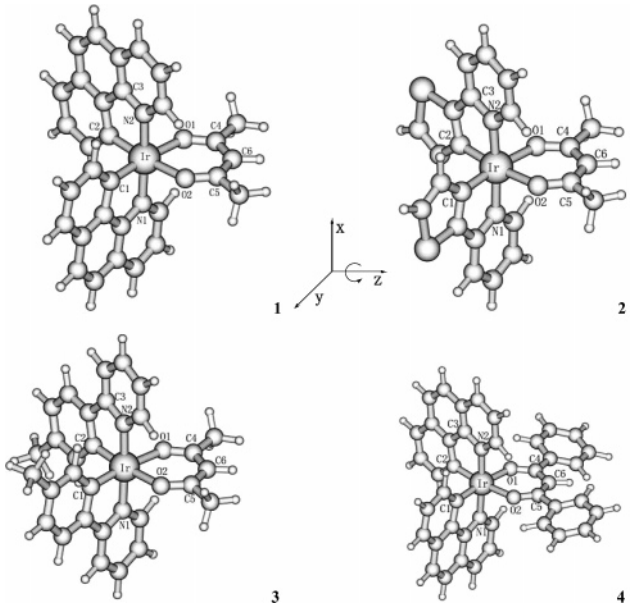

Figure 1. Optimized geometry structures of **1**−**4** at the B3LYP/LANL2DZ level.

Computational Details and Theory

The calculated complexes display C_2 symmetry in both the ground and excited states. As shown in Figure 1, the z/C_2 axis is oriented through Ir and the central C(6) atom in the acac cycle, and the *x* and *y* axes both deviate 45° from the acac plane. The three ligands are almost perpendicular to each other. The DFT-B3LYP (density functional method)[22] and CIS (configuration interaction with single excitations) approaches[23] have been employed to optimize the geometry structures in the ground and excited states, respectively. On the basis of the optimized geometry structures in the ground and excited states, the absorption and emission properties in tetrahydrofuran (THF) media can be calculated by time-dependent density functional theory (TDDFT)[24] associated with the polarized continuum model (PCM).[25] This kind of theoretical approach has been proven to be reliable for transition-metal complex systems. McCusker et al.[26] employed the B3LYP method to study the excited-state electronic structures of [RuL$_2$-(NCS)$_2$]$^{4-}$ (L = 4,4′-dicarboxylato-2,2′-bipyridine); Yang et al.[27] presented a combined DFT (B3LYP), CIS, and TDDFT solution to predict the absorptions and emissions of M(CO)$_4$(phen) (M = Cr, Mo, W; phen = 1,10-phenanthroline).

In the calculations, the quasi-relativistic pseudo-potentials of Ir atoms proposed by Hay and Wadt[28] with 17 valence electrons were employed, and LANL2DZ basis sets associated with the pseudo-potential were adopted. The basis sets were described as Ir (8s6p3d/3s3p2d), C and N (10s5p/3s2p), and H (4s/2s). Thus, 383 basis functions and 256 electrons for **1**, 319 basis functions and 216

(15) Lamansky, S.; Djurovich, P.; Murphy, D.; Abdel-Razzaq, F.; Kwong, R.; Tsyba, I.; Bortz, M.; Mui, B.; Bau, R.; Thompson, M. E. *Inorg. Chem.* **2001**, *40*, 1704.
(16) Hay, P. J. *J. Phys. Chem. A* **2002**, *106*, 1634.
(17) (a) Markham, J. P. J.; Lo, S.-C.; Magennis, S. W.; Burn, P. L.; Samuel, I. D. W. *Appl. Phys. Lett.* **2002**, *80*, 2645. (b) Adachi, C.; Baldo, M. A.; Forrest, S. R. *Appl. Phys. Lett.* **2000**, *77*, 904. (c) Colombo, M. G.; Gudel, H. U. *Inorg. Chem.* **1993**, *32*, 3081. (d) Baldo, M. A.; Lamansky, S.; Burrows, P. E.; Thompson, M. E.; Forrest, S. R. *Appl. Phys. Lett.* **1999**, *75*, 4.
(18) Ostrowski, J. C.; Robinson, M. R.; Heeger, A. J.; Bazan, G. C. *Chem. Commun.* **2002**, 784.
(19) King, K. A.; Spellane, P. J.; Watts, R. J. *J. Am. Chem. Soc.* **1985**, *107*, 1431.
(20) (a) Wilde, A. P.; King, K. A.; Watts, R. J. *J. Phys. Chem.* **1991**, *95*, 629. (b) Ohsawa, Y.; Sprouse, S.; King, K. A.; DeArmond, M. K.; Hanck, K. W.; Watts, R. J. *J. Phys. Chem.* **1987**, *91*, 1047. (c) Dedeian, K.; Djurovich, P. I.; Garces, F. O.; Carlson, G.; Watts, R. J. *Inorg. Chem.* **1991**, *30*, 1685. (d) Colombo, M. G.; Brunold, T. C.; Riedener, T.; Güdel, H. U. *Inorg. Chem.* **1994**, *33*, 545.
(21) (a) Hwang, F.-M.; Chen, H.-Y.; Chen, P.-S.; Liu, C.-S.; Chi, Y.; Shu, C.-F.; Wu, F.-I.; Chou, P.-T.; Peng, S.-M.; Lee, G.-H. *Inorg. Chem.* **2005**, *44*, 1344. (b) Namdas, E. B.; Ruseckas, A.; Samuel, I. D. W.; Lo, S.-C.; Burn, P. L. *J. Phys. Chem. B* **2004**, *108*, 1570. (c) Laskar, I. R.; Chen, T.-M. *Chem. Mater.* **2004**, *16*, 111. (d) Bhalla, G.; Oxgaard, J.; Goddard, W. A., III; Periana, R. A. *Organometallics* **2005**, *24*, 3229. (e) Runge, E.; Gross, E. K. U. *Phys. Rev. Lett.* **1984**, *52*, 997.
(22) Runge, E.; Gross, E. K. U. *Phys. Rev. Lett.* **1984**, *52*, 997.
(23) (a) Stanton, J. F.; Gauss, J.; Ishikawa, N.; Head-Gordon, M. *J. Chem. Phys.* **1995**, *103*, 4160. (b) Foreman, J. B.; Head-Gordon, M.; Pople, A. *J. Phys. Chem.* **1992**, *96*, 135. (c) Waiters, V. A.; Hadad, C. M.; Thiel, Y.; Colson, S. D.; Wibergy, K. B.; Johnson, P. M.; Foresman, J. B. *J. Am. Chem. Soc.* **1991**, *113*, 4782.
(24) (a) Stratmann, R. E.; Scuseria, G. E. *J. Chem. Phys.* **1998**, *109*, 8218. (b) Matsuzawa, N. N.; Ishitani, A. *J. Phys. Chem. A* **2001**, *105*, 4953. (c) Casida, M. E.; Jamorski, C.; Casida, K. C.; Salahub, D. R. *J. Chem. Phys.* **1998**, *108*, 4439.
(25) (a) Cossi, M.; Scalmani, G.; Regar, N.; Barone, V. *J. Chem. Phys.* **2002**, *117*, 43. (b) Barone, V.; Cossi, M. *J. Chem. Phys.* **1997**, *107*, 3210.
(26) Monat, J. E.; Rodriguez, J. H.; McCusker, J. K. *J. Phys. Chem. A* **2002**, *106*, 7399.
(27) Yang, L.; Feng, J.-K.; Ren, A.-M. *Synth. Met.* **2005**, *152*, 265.
(28) (a) Hay, P. J.; Wadt, W. R. *J. Chem. Phys.* **1985**, *82*, 299. (b) Hay, P. J.; Wadt, W. R. *J. Chem. Phys.* **1985**, *82*, 270.

Table 1. Main Optimized Geometry Structural Parameters of the Complexes in the Ground and Lower Lying Triplet Excited States at the B3LYP and CIS Levels, Respectively, Together with the Experimental Values of 3

	1		2		3		4		
param	X^1A	A^3A	X^1A	A^3B	X^1A	A^3B	X^1A	A^3B	**3** exptl[a]
				Bond Lengths (Å)					
Ir−N(1)	2.063	2.095	2.070	2.100	2.054	2.085	2.063	2.095	2.040(5)
Ir−C(1)	2.017	2.044	2.003	2.031	2.010	2.036	2.018	2.044	1.985(7)
Ir−O(1)	2.184	2.168	2.175	2.163	2.192	2.180	2.174	2.161	2.161(4)
C(4)−O(1)	1.305	1.278	1.305	1.279	1.304	1.278	1.308	1.280	
				Bond Angles (deg)					
N(1)−Ir−N(2)	175.9	176.2	177.3	175.9	177.0	176.6	176.9	176.3	176.2(2)
O(1)−Ir−O(2)	85.8	83.0	85.9	83.3	85.3	82.6	85.4	82.3	88.2(2)
C(1)−Ir−C(2)	92.3	91.5	93.4	91.7	92.6	91.6	92.6	91.4	
				Dihedral Angles (deg)					
C(3)−N(2)−Ir−O(1)	88.2	90.7	86.6	90.2	87.1	90.3	88.0	91.2	
C(3)−N(2)−Ir−C(1)	94.5	93.0	96.5	93.4	95.9	93.6	95.0	92.8	

[a] From ref 15.

electrons for **2**, 373 basis functions and 248 electrons for **3**, and 481 basis functions and 320 electrons for **4** have been included in the calculations. All of the calculations were accomplished by using the Gaussian 03 software package[29] on an Origin/3800 server.

Results and Discussion

Geometry Structures in the Ground State and Absorptions in THF Media. The calculated results reveal that all of the complexes have the X^1A ground state. The main optimized geometry structural parameters in the ground state together with the X-ray crystal diffraction data of **3**[15] are given in Table 1, and the optimized structures are shown in Figure 1. The optimization results show that the three ligands are almost perpendicular to each other with C(3)−N(2)−Ir−O(1) and C(3)−N(2)−Ir−C(1) dihedral angles close to 90°. Furthermore, it can be seen that the optimized bond lengths and bond angles of all the complexes in the ground state are in general agreement with the corresponding experimental values of **3**. The calculated bond distances of Ir−N (2.054 Å), Ir−C (2.010 Å), and Ir−O (2.192 Å) are overestimated by about 0.01−0.03 Å in comparison with the measured values. The calculated bond angles are closed to the experimental values, except that the O(1)−Ir−O(2) bond angle (85.3°) deviates slightly (2.9°) from the experimental value. The discrepancy of the geometry structural data between the calculated and measured values is reasonable and acceptable, since the environments of the complexes are different in the two cases: in the latter complex, the molecule is in a tight crystal lattice, while in the former complex, the molecule is free.

The calculated absorptions in the UV−visible region associated with their oscillator strengths, the main configurations and their assignments, and the experimental results are summarized in Table 2; the frontier molecular orbital compositions of **1** and **4** are compiled in Tables 3 and 4, respectively, while those of **2** and **3** are shown in Tables S1 and S2 (Supporting Information). Fitted Gaussian type absorption curves with the calculated absorption data are shown in Figure 2. To intuitively understand the transition process, the molecular orbital energy levels involved in transitions of **1**−**4** are displayed in Figure 3.

Figure 2 shows there are distinguishable absorption bands at 450−500 nm (2.76−2.48 eV), 430−490 nm (2.88−2.53 eV), 420−470 nm (2.95−2.64 eV), and 460−510 nm (2.70−2.43 eV) for **1**−**4**, respectively. Indeed, these low-energy absorption bands for **1**−**3** are overlapped ones, since both of the first two low-energy transitions are responsible for the absorption bands, but with a small energy gap (0.03−0.10 eV) and large disparity in magnitude of oscillation strength (one is larger than 0.03, and the other is smaller than 0.004) (see Table 2). For complex **1**, the excitation of MO 65a → MO 64b dominates the absorption band between 450 and 500 nm. Table 3 shows that MO 65a (HOMO) is composed of 29% d_{z^2}(Ir), 10% $d_{x^2-y^2}$(Ir), and 47% π(bzq), while MO 64b is the π^*(bzq) type orbital. Furthermore, another contributing transition with low oscillation strength value (0.0064) is mainly from MO 65a → MO 66a, in which MO 66a is also a π^*(bzq) orbital with a composition of 96.3%. Therefore, this absorption band can be assigned to the combination of MLCT (metal to ligand charge transfer) and ILCT (intraligand charge transfer) transitions {[d_{z^2}(Ir) + $d_{x^2-y^2}$(Ir) + π(bzq)] → [π^*(bzq)]}. In the meanwhile, the low-energy absorption bands at 430−490, 420−470, and 460−510 nm for complexes **2**−**4** have transition paths similar to that at 450−500 nm of **1**. Thus, the above low-energy absorptions of **1**−**4** can be described as a {[d_{z^2}(Ir) + $d_{x^2-y^2}$(Ir) + π(C^N)] → [π^*-(C^N)}] transition with MLCT/ILCT character (see Figure 4). Different from the others, complex **4** shows an extra lower energy weak absorption at 536 nm, in which the MO 81a → MO 82a excitation mainly contributes to the transition, which can be attributed to {[d_{z^2}(Ir) + $d_{x^2-y^2}$(Ir) + π(bzq)] → [π^*-(dbm)]} with MLCT/LLCT (ligand to ligand charge-transfer transition) character (see Table 4). In comparison with the analogue **1**, this lower lying absorption of **4** is unusual. The intense participation of a conjugating phenyl group remarkably stabilizes the molecular orbital. Hence, the frontier molecular orbitals are affected by the phenyl group. In addition, there is an absorption at 439 nm for **4** and the excitation of MO 79b → MO 82a (|CI| = 0.665 98) corresponds to the transition and can be described as a {[d_{xz}(Ir) + d_{yz}(Ir) + π(dbm)] → [π^*-(dbm)]} transition. The above low-energy absorption bands for the complexes **1**−**3** can be regarded as the measured absorptions at 430−520 nm (2.88−2.38 eV), 430−470 nm (2.88−2.69 eV),

(29) Frisch, M. J.; Trucks, G. W.; Schlegel, H. B.; Scuseria, G. E.; Robb, M. A.; Cheeseman, J. R.; Montgomery, J. A., Jr.; Vreven, T.; Kudin, K. N.; Burant, J. C.; Millam, J. M.; Iyengar, S. S.; Tomasi, J.; Barone, V.; Mennucci, B.; Cossi, M.; Scalmani, G.; Rega, N.; Petersson, G. A.; Nakatsuji, H.; Hada, M.; Ehara, M.; Toyota, K.; Fukuda, R.; Hasegawa, J.; Ishida, M.; Nakajima, T.; Honda, Y.; Kitao, O.; Nakai, H.; Klene, M.; Li, X.; Knox, J. E.; Hratchian, H. P.; Cross, J. B.; Bakken, V.; Adamo, C.; Jaramillo, J.; Gomperts, R.; Stratmann, R. E.; Yazyev, O.; Austin, A. J.; Cammi, R.; Pomelli, C.; Ochterski, J. W.; Ayala, P. Y.; Morokuma, K.; Voth, G. A.; Salvador, P.; Dannenberg, J. J.; Zakrzewski, V. G.; Dapprich, S.; Daniels, A. D.; Strain, M. C.; Farkas, O.; Malick, D. K.; Rabuck, A. D.; Raghavachari, K.; Foresman, J. B.; Ortiz, J. V.; Cui, Q.; Baboul, A. G.; Clifford, S.; Cioslowski, J.; Stefanov, B. B.; Liu, G.; Liashenko, A.; Piskorz, P.; Komaromi, I.; Martin, R. L.; Fox, D. J.; Keith, T.; Al-Laham, M. A.; Peng, C. Y.; Nanayakkara, A.; Challacombe, M.; Gill, P. M. W.; Johnson, B.; Chen, W.; Wong, M. W.; Gonzalez, C.; Pople, J. A. *Gaussian 03*, revision C.02; Gaussian, Inc.: Wallingford, CT, 2004.

Table 2. Absorptions of 1−4 Calculated with the TDDFT Method, Together with the Experimental Values

	transition	confign (CI coeff)	*E*/nm (eV)	oscillator	assignt	λ_{exptl} (nm)[a]
		Singlet → Singlet				
1	$X^1A \rightarrow A^1A$	65a → 66a (0.687 86)	484 (2.56)	0.0064	MLCT/ILCT	500
	$X^1A \rightarrow B^1A$	65a → 64b (0.683 30)	480 (2.59)	0.0314	MLCT/ILCT	470
	$X^1A \rightarrow C^1B$	63b → 66a (0.675 91)	415 (2.99)	0.0514	MLCT/LLCT	
	$X^1A \rightarrow D^1B$	64a → 64b (0.612 33)	364 (3.40)	0.1535	MLCT/ILCT	360
	$X^1A \rightarrow E^1A$	62a → 66a (0.509 35)	286 (4.33)	0.0551	ILCT/MLCT	260
		62b → 65b (0.316 98)			ILCT	
2	$X^1A \rightarrow A^1B$	55a → 54b (0.671 98)	462 (2.69)	0.1063	MLCT/ILCT	453
	$X^1A \rightarrow B^1A$	55a → 56a (0.667 23)	445 (2.79)	0.0025	MLCT/ILCT	
	$X^1A \rightarrow C^1B$	53b → 56a (0.673 53)	389 (3.18)	0.0392	MLCT/LLCT	387
	$X^1A \rightarrow D^1B$	54a → 54b (0.582 75)	346 (3.58)	0.1052	MLCT/ILCT	336
		53b → 57a (0.276 96)			MLCT/LLTC	
	$X^1A \rightarrow E^1B$	52b → 58a (0.468 17)	283 (4.38)	0.3523	ILCT	302
		51b → 56a (0.315 56)			LLCT/ILCT	
3	$X^1A \rightarrow A^1B$	63a → 62b (0.684 39)	452 (2.74)	0.0475	MLCT/ILCT	495
	$X^1A \rightarrow B^1A$	63a → 64a (0.684 51)	446 (2.78)	0.0019	MLCT/ILCT	460
	$X^1A \rightarrow C^1B$	61b → 64a (0.667 40)	388 (3.19)	0.0399	MLCT/LLCT	410
	$X^1A \rightarrow D^1B$	62a → 62b (0.476 39)	352 (3.52)	0.0737	MLCT/ILCT	370
		61b → 65a (−0.452 11)			MLCT/ILCT	
	$X^1A \rightarrow E^1B$	63a → 64b (0.484 10)	279(4.44)	0.1616	MLCT/ILCT	270
		60b → 66a (0.391 35)			ILCT	
4	$X^1A \rightarrow A^1A$	81a → 82a (0.697 06)	536 (2.31)	0.0035	MLCT/LLCT	
	$X^1A \rightarrow B^1B$	81a → 80b (0.682 86)	477 (2.60)	0.0310	MLCT/ILCT	
	$X^1A \rightarrow C^1B$	79b → 82a (0.665 98)	439 (2.82)	0.0460	MLCT/ILCT	
	$X^1A \rightarrow D^1A$	80a → 82a (0.663 98)	390 (3.18)	0.1328	MLCT/LLCT	
	$X^1A \rightarrow E^1B$	77b → 82a (0.511 55)	331 (3.75)	0.2506	MLCT/ILCT	
		75b → 82a (0.394 68)			LLCT	
	$X^1A \rightarrow F^1A$	78a → 83a (0.430 97)	287 (4.32)	0.1080	MLCT	
		78b → 81b (−0.333 09)			LLCT/ILCT	
		Singlet → Triplet				
1	$X^1A \rightarrow A^3A$	65a → 66a (0.664 25)	529 (2.34)		MLCT/ILCT	
2	$X^1A \rightarrow A^3B$	55a → 54b (0.657 41)	572 (2.17)		MLCT/ILCT	
3	$X^1A \rightarrow A^3B$	63a → 62b (0.661 91)	496 (2.50)		MLCT/ILCT	
4	$X^1A \rightarrow A^3B$	79b → 82a (0.689 09)	564 (2.20)		MLCT/ILCT	
		Ligands (Singlet → Singlet)				
bzq	$X^1A \rightarrow A^1A'$	6a″ → 8a″(0.551 62)	292 (4.25)	0.1095	$\pi \rightarrow \pi^*$	
thp	$X^1A \rightarrow A^1A'$	5a″ → 7a″ (0.558 01)	269 (4. 62)	0.1331	$\pi \rightarrow \pi^*$	
tpy	$X^1A \rightarrow A^1A$	43a → 46a (0.608 93)	268 (4.62)	0.2731	$\pi \rightarrow \pi^*$	
acac	$X^1A \rightarrow A^1A''$	15a′ → 3a″ (0.613 33)	255 (4.86)	0.5030	$\pi \rightarrow \pi^*$	
dbm	$X^1A \rightarrow A^1B_2$	$10b_1 \rightarrow 11a_2$ (0.537 84)	257 (4.82)	0.5227	$\pi \rightarrow \pi^*$	

[a] From ref 8.

Table 3. Molecular Orbital Compositions in the Ground State for Ir(bzq)2(acac) (1) at the B3LYP Level

orbital	energy (eV)	MO composition (%) Ir	bzq	acac	main bond type	Ir component
65b	−1.1666	0.8	98.2	1.0	π^*(bzq)	
64b	−1.7829	3.1	96.3	0.6	π^*(bzq)	
66a	−1.8294	2.2	96.3	1.5	π^*(bzq)	
		HOMO−LUMO Energy Gap				
65a	−5.0578	45.6	47.3	7.1	d(Ir) + π(bzq)	28.9 d_{z^2}, 9.3 $d_{x^2-y^2}$
63b	−5.521	44.5	17.4	38.1	d(Ir) + π(bzq) + π(acac)	21.1 $d_{xz} + d_{yz}$, 17.5 d_{xy}
62b	−5.8818	1.8	94.4	3.8	π(bzq)	
64a	−5.9191	61.2	34.3	4.5	d(Ir) + π(bzq)	60.6 $d_{yz} + d_{xz}$
61b	−6.3545	7.7	58.6	33.7	π(bzq) + π(acac)	
63a	−6.4372	22.4	73.2	4.4	d(Ir) + π(bzq)	
60b	−6.6527	9.5	49.1	41.4	π(bzq) + π(acac)	
62a	−6.6848	17.1	71.6	11.3	d(Ir) + π(bzq) + π(acac)	9.2 d_{z^2}

Table 4. Molecular Orbital Compositions in the Ground State for Ir(bzq)2(dbm) (4) at the B3LYP Level

orbital	energy (eV)	MO composition (%) Ir	bzq	dbm	main bond type	Ir component
81b	−1.1657	0.7	97.7	1.6	π^*(bzq)	
80b	−1.7791	3.1	96.1	0.8	π^*(bzq)	
83a	−1.809	3.7	89.3	7.0	π^*(bzq)	
82a	−2.0713	1.8	16.3	81.9	π^*(dbm) + π(bzq)	
		HOMO−LUMO Energy Gap				
81a	−5.0657	45.0	47.4	7.6	d(Ir) + π(bzq)	28.6 d_{z^2}, 13.1 $d_{x^2-y^2}$
79b	−5.5427	43.7	18.4	37.9	d(Ir) + π(bzq) + π(dbm)	37.9 $d_{xz} + d_{yz}$
78b	−5.8889	2.2	93.5	4.3	π(bzq)	
80a	−5.9139	59.4	32.7	7.9	d(Ir) + π(bzq)	50.6 d_{xy}
77b	−6.2905	13.6	38.1	48.3	π(bzq) + π(dbm)	
79a	−6.4309	19.8	74.5	5.7	π(bzq)	
76b	−6.5901	15.9	63.3	20.8	d(Ir) + π(bzq) π(dbm)	
78a	−6.6802	16.9	68.9	14.2	d(Ir) + π(bzq) + π(dbm)	
75b	−6.8263	4.0	36.2	59.8	π(bzq) + π(dbm)	

and 430−500 nm (2.88−2.48 eV) for **1**−**3**, respectively, which have been assigned to a mixture of singlet and triplet MLCT transitions.[8]

Other calculated differential absorptions are at 415 nm (2.99 eV), 389 nm (3.18 eV), and 388 nm (3.19 eV) for **1**−**3**, respectively. These absorptions have a combined MLCT/LLCT character (see Tables S1 and S2) and are attributed to the {[d_{xz}-(Ir) + d_{yz}(Ir) + d_{xy}(Ir) + π(LX)] → [π^*(C^N)]} transition. With respect to **4**, a MLCT/LLCT type transition at 390 nm is described as {[d_{xy}(Ir) + π(C^N)] → [π^*(LX)]} (see Table 4). For these absorption bands, the different transition character of **4** in comparison to those of **1**−**3** is also due to the introduction of phenyl groups on the acac fragment in **4**, which results in the enhancement of the π-conjugated effects and π-accepting abilities of the acac fragment.

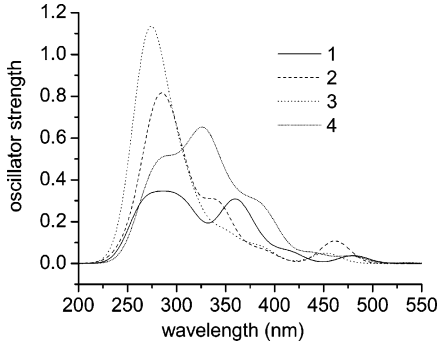

Figure 2. Simulated absorption spectra of **1**−**4** in THF media with the calculated data at the TD-B3LYP/LANL2DZ level.

The other higher energy absorptions in the UV−visible region have ILCT and/or LLCT character. However, this type of transition is perturbed by the MLCT components. Indeed, the participation of the MLCT components in the UV−visible region absorption is usual and is even more remarkable in the lower energy absorption bands. This point can be seen from the large compositions of metal atom in the lower energy absorption bands. Calculations on the isolated ligands bzq, thp, tpy, acac and dbm showed that the intraligand $\pi \rightarrow \pi^*$ transitions occur at $\lambda < 300$ nm (see Table 2). Therefore, the coordination interaction between the metal and the ligands produce lower energy absorptions and, due to the presence of the metal, spin-forbidden singlet−triplet transitions are likely to be observed. The calculated vertical triplet absorptions of the complexes at 529 nm (2.34 eV), 572 nm (2.17 eV), 496 nm (2.50 eV), and 564 nm (2.20 eV) for complexes **1**−**4**, respectively, have an evident MLCT nature (see Table 2). Experimentally, the lower energy ^{1}MLCT and ^{3}MLCT transitions cannot be resolved clearly. As seen in Ir(bzq)$_2$(acac), there is a broad absorption band at 430−520 nm (2.88−2.38 eV),[15] where combined ^{1}MLCT and ^{3}MLCT transitions are responsible for it.

Therefore, our theoretical investigation demonstrates that the MLCT transitions in these kinds of Ir(III) complexes dominate the low-energy-region absorption spectra. We think this is the most fascinating factor for the complexes as the emissive candidates. On one hand, this kind of transition is dipole-allowed; on the other hand, the singlet−triplet transition probably occurs due to the participation of the metal. Both of these two properties can ensure the high luminescence efficiency of the complexes.

Correlation of the Absorption and the Ligands. In comparison with those of **1**, the absorptions of **2** and **3** are blue-shifted to some extent (see Figure 2). This is due to the weaker π-conjugation effects and π-accepting abilities of the thp and tpy in **2** and **3** compared to those of bzq in **1**, so that the HOMO−LUMO energy gaps of **2** and **3** are larger. In contrast, the lower energy absorptions of **4** are dramatically red-shifted (0.25 eV) relative to those of its analogue **1**. The lower lying

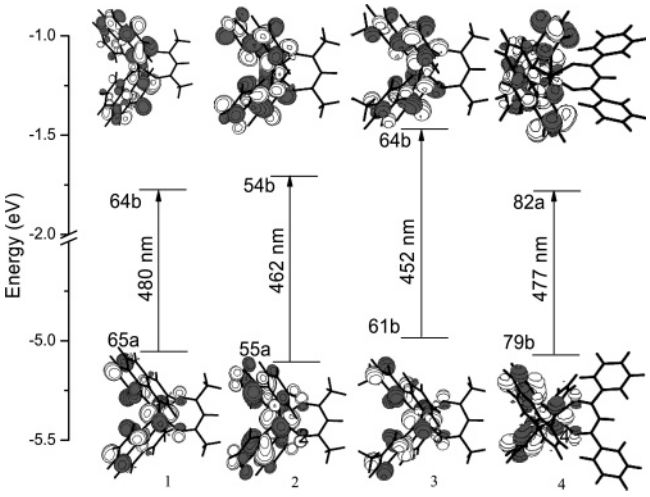

Figure 4. Transitions contributing to the absorptions at 480, 462, 452, and 477 nm for **1**−**4**, respectively, in THF media.

absorption energies are in the order **3** > **2** > **1** > **4**, which is just the reverse of the π-conjugation effect of the complex in the order **3** < **2** < **1** < **4**. The introduction of a phenyl group on the acac fragment enhances the conjugation effect and significantly lowers the LUMO energy level, resulting in the considerable decrease of the HOMO−LUMO energy gap of **4** (see Figure 3).

Geometry Structures in the Triplet Excited State and Emissions in the THF Media. The main geometry structural parameters of the complexes in the A^3A (**1** and **4**) and A^3B (**2** and **3**) excited states obtained by the CIS method are given in Table 1. In the low-lying triplet excited state the geometry structures of **1**−**4** do not vary notably relative to those in the ground state, except that the Ir−N, Ir−C, and Ir−O bond lengths change slightly and the four complexes show similar variation trends. The calculated Ir−C and Ir−N bond lengths relax by about 0.03 Å, but the Ir−O and the C(4)−O(1) bond lengths

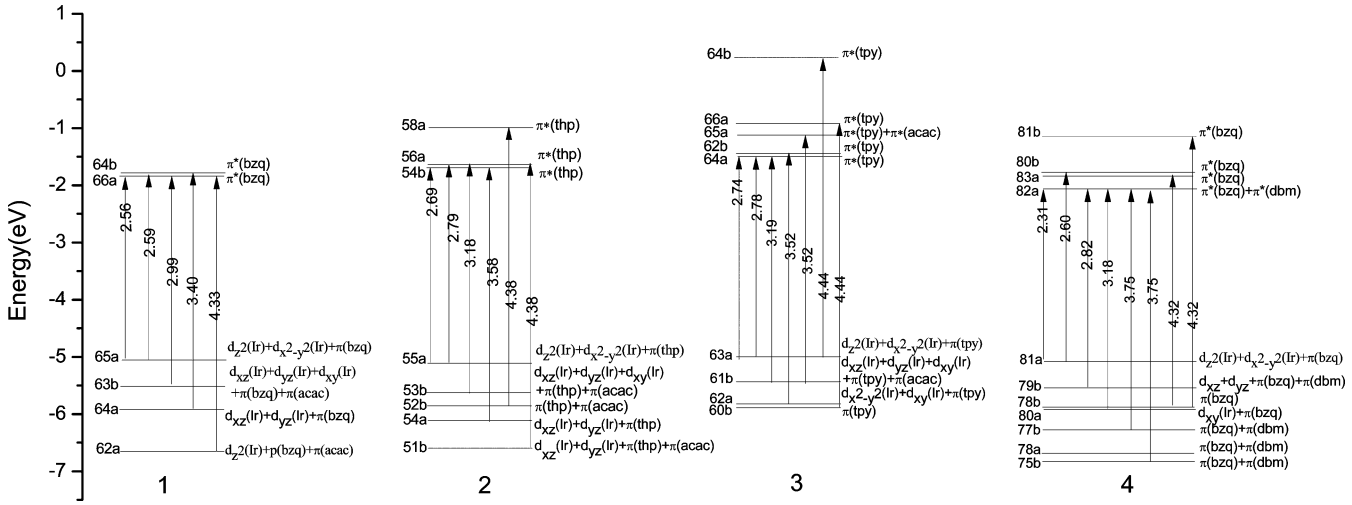

Figure 3. Diagrams of the molecular orbitals related to the absorptions for **1**−**4**.

Table 5. Phosphorescent Emissions of 1−4 Calculated with the TDDFT Method, Together with the Corresponding Experimental Values

	transition	confign (CI coeff)	*E*/nm (eV)	assignt	exptl/nm (eV)[a]
1	$A^3A \rightarrow X^1A$	66a → 65a (0.627 78)	541 (2.29)	^{3}MLCT/^{3}ILCT	548 (2.26)
2	$A^3B \rightarrow X^1A$	54b → 55a (0.653 25)	589 (2.11)	^{3}ILCT/^{3}MLCT	562 (2.20)
3	$A^3B \rightarrow X^1A$	62b → 63a (0.649 50)	499 (2.48)	^{3}MLCT/^{3}ILCT	512 (2.42)
4	$A^3A \rightarrow X^1A$	82a → 81a (0.449 62) 83a → 81a (−0.443 21)	540 (2.29)	^{3}MLCT/^{3}ILCT	

[a] From ref 8.

Table 6. Molecular Orbital Compositions in the A^3A Excited States for Ir(bzq)$_2$(acac) (1) at the B3LYP Level

orbital	energy (eV)	MO composition (%) Ir	bzq	acac	main bond type	Ir component (%)
64b	−1.7677	2.2	97.3	0.5	π*(bzq)	
66a	−1.8025	1.7	97.6	0.7	π*(bzq)	
		HOMO−LUMO Energy Gap				
65a	−5.0132	47.1	43.9	9.0	d(Ir) + π(bzq)	29.7 d_{z^2}, 10.2 $d_{x^2-y^2}$
63b	−5.4382	43.5	15.0	41.5	d(Ir) + π(bzq) + π(acac)	20.9 d_{yz} + d_{xz}, 17.1 d_{xy}
62b	−5.8339	1.6	93.3	5.1	π(bzq)	

Table 7. Molecular Orbital Compositions in the A^3A Excited States for Ir(bzq)$_2$(dbm) (4) at the B3LYP Level

orbital	energy (eV)	MO composition (%) Ir	bzq	dbm	main bond type	Ir component
83a	−1.7698	3.8	71.8	24.4	π*(bzq) + π*(dbm)	
80b	−1.7707	2.2	97.3	0.5	π*(bzq)	
82a	−1.8896	0.7	33.7	65.6	π*(bzq) + π*(dbm)	
		HOMO−LUMO Energy Gap				
81a	−5.0254	46.6	44.1	9.3	d(Ir) + π(bzq)	29.3 d_{z^2}, 14.4 $d_{x^2-y^2}$

strengthen by about 0.02 Å. The calculated O(1)−Ir−O(2) bond angle reduces by 2.0−3.0°, while the C(3)−N(2)−Ir−O(1) and C(3)−N(2)−Ir−C(1) dihedral angles change by 1.5−4.0°. The slight changes of the geometry structural parameters result from the electron transfer from the Ir−C^N bonding orbital to the π*(C^N or LX) orbital (vide infra) upon excitation.

The calculated frequencies of Ir−N, Ir−C, Ir−O, and C−O in the ground and excited states are in accordance with the variation of the geometry parameters. In complex **1**, for example, the ν(Ir−N) stretching frequency appears at 670 and 666 cm^{-1} in the ground and excited states, respectively. The reduction of the Ir−N stretching frequency in the excited state indicates the weakness of the Ir−N bonding interaction, which is consistent with the lengthening of the Ir−N bond distance in the excited state. The variation of the ν(Ir−C) stretching frequency is similar to the case for ν(Ir−N). In contrast, the Ir−O and C(4)−O(1) stretching frequencies are somewhat enlarged in the excited state (423, 1663 cm^{-1}) relative to those in the ground state (418, 1565 cm^{-1}), being in line with the shortening of the Ir−O and C(4)−O(1) bond lengths in the excited state. Complexes **2**−**4** display changes similar to those for **1**. Similar vibration characteristics have also been found for [OsN(C≡CH)$_4$];[30] the Os≡N bond is lengthened in the excited state compared to that in the ground state, which is in agreement with the lower vibration frequency of ν(Os−N) (∼780 cm^{-1}) in the excited state as compared to that (∼1175 cm^{-1}) in the ground state.

The calculated phosphorescence of **1**−**4** in THF media and the measured emission in 2-methyltetrahydrofuran solution are summarized in Table 5; the frontier molecular orbital compositions responsible for the emissions are compiled in Tables 6 and 7 and in Tables S3 and S4 (Supporting Information).

The calculated phosphorescences at 541 nm (2.29 eV), 589 nm (2.11 eV), and 499 nm (2.48 eV) for **1**−**3** agree well with their respective experimental values[8] at 548 nm (2.26 eV), 562 nm (2.21 eV) and 512 nm (2.42 eV). For **1**, the excitation MO 66a → MO 65a has the largest configuration coefficient (0.627 78) and causes the emission. The analysis of the transition reveals that the emission originates from the ^{3}{[d_{z^2}(Ir) + $d_{x^2-y^2}$(Ir) + π(bzq)][π*(bzq)]} excited state with MLCT/ILCT character (see Table 6). Figure 5 displays an intuitive electron transition diagram of the emission. Experimentally, the measured phosphorescence of **1** at 548 nm (2.26 eV)[8] in 2-methyltetrahydrofuran media has been tentatively assigned to a ^{3}MLCT emission.

The nature of the phosphorescence of **2** and **3** are similar to that of **1** (see Tables S3 and S4), which are all attributed to a ^{3}ILCT/^{3}MLCT ^{3}{[d_{z^2}(Ir) + $d_{x^2-y^2}$(Ir) + π(C^N)][π*(C^N)]} emission. The ^{3}ILCT component in **2** is more significant than those in **1** and **3**, because the compositions of the C^N ligands (thp 53.5%) in the HOMO of **2** are more than those of the bzq (43.9%) and tpy (40.1%) ligands in **1** and **3**. Experimentally the emission of **2** has been found to originate from the ^{3}{[π-(C^N) + d(Ir)][π*(C^N)]} excited state.[8] For **4**, not only the C^N ligand but also the LX ligand correlates with the emission. The emission of **4** at 540 nm should come from the ^{3}{[d_{z^2}(Ir) + $d_{x^2-y^2}$(Ir) + π*(bzq)][π*(bzq) + π*(dbm)]} excited state. Herein, we note that the C^N ligands have a great effect on the phosphorescence for **1**−**3** but the emission of **4** hardly shifts with changes of the LX ligands compared with the emission for complex **1**, which confirms the conclusion obtained by Thompson[15] and co-workers that changes in the C^N ligand have a marked effect on the phosphorescence spectrum while changes in the LX ligand lead to a relatively minor shift.

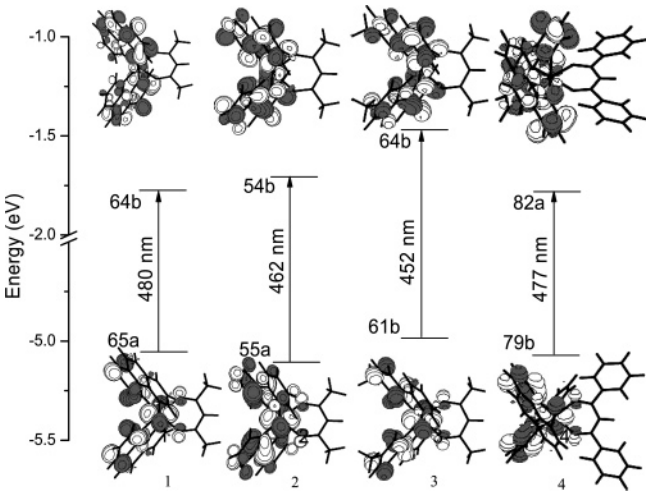

Figure 5. Transitions responsible for the emissions at 541, 589, 499, and 540 nm for **1**−**4**, respectively, simulated in THF media.

(30) Zhang, Y.-H.; Xia, B.-H.; Pan, Q.-J.; Zhang, H.-X. *J. Chem. Phys.* **124**, 144309.

The above discussion reveals that the lower lying absorptions calculated at 484, 462, 452, and 536 nm for **1**−**4**, respectively, dominantly arise from the combination of MLCT and ILCT or LLCT electronic transitions, while the calculated phosphorescence is just the reverse process of these lower lying absorptions. The energy differences between the calculated lower energy absorptions and the phosphorescence are 0.27, 0.58, and 0.26 eV for **1**−**3**, respectively, while the measured Stokes shifts of the complexes are 0.38, 0.44, and 0.37 eV for **1**−**3**, respectively.[8] Therefore, the calculated Stokes shifts are reasonable.

Many researchers have speculated that there is a competition between the MLCT and [$\pi \rightarrow \pi^*$] ligand-centered (LC) transitions due to the very close energy levels of the terminal orbitals in the complexes.[31] According to our studies, the calculated combined MLCT/LC (ligand-centered) transition nature of the absorptions in the UV−visible region confirms the prediction. Furthermore, we note that the metal 5d(Ir) composition ranges from 40% to 51% with an almost equal admixture of π(C^N) in the HOMOs for **1**−**4**, while the LUMOs are mainly populated on C^N for **1**−**3** but on LX for **4**. Therefore, the calculation results indicate that there is a competition between different types of ^{3}MLCT transitions: one type only concentrates on the C^N ligands, and the other type relates to both the C^N and LX ligands, and which one will win the competition depends on the π-conjugation effects and electron-accepting abilities of the ligands. Hay[16] came to a similar conclusion, that two types of ^{3}MLCT involve a π^* orbital on the C^N or LX ligands. In addition, our calculation results indicate that there is a third type of ^{3}MLCT involving a mixture of π^* orbitals on the C^N and LX ligands and the competitions result from the π-conjugation effects of the different ligand.

Obviously, the phosphorescent excited state is relevant to both the metal and the ligands, and the intense interaction between the metal and the ligands in the frontier molecular orbitals leads to the spin-forbidden LC transition. The calculated metal compositions in the HOMOs of **1**−**3** are 47.1%, 40.0%, and 51%, respectively (see Table 6 and Tables S3 and S4), while their respective measured quantum efficiencies are 0.27, 0.12 and 0.31,[8] in which they have the same trend in both the metal composition and quantum efficiency on the order of **2** < **1** < **3**. Therefore, more metal components in the frontier molecular orbital can make the spin-forbidden transition more possible. We think this could be a guiding principle to design new phosphorescent materials.

(31) (a) Feliz, M.; Ferraudi, G. *Inorg. Chem.* **1998**, *37*, 2806. (b) Chanda, N.; Sarkar, B.; Kar, S.; Fiedler, J.; Kaim, W.; Lahiri, G. K. *Inorg. Chem.* **2004**, *43*, 5128. (c) Lewis, J. D.; Perutz, R. N.; Moore, J. N. *J. Phys. Chem. A* **2004**, *108*, 9037.

Conclusions

The present work theoretically investigated the geometry structures, absorptions, and phosphorescent properties of four iridium(III) cyclometalated complexes. The calculation reveals that the MLCT transition is present in all UV−visible regions along with the LC (ligand-centered) transition and this is the decisive factor for the spin-forbidden electron transition to occur. Furthermore, the large metal compositions in the frontier molecular orbitals can bring about high quantum efficiency. In addition, the π-conjugated C^N ligands can effectively influence the emission color. It is very practical to explore the relationship between the d−π interaction and the phosphorescent properties of the metal complexes. We hope these theoretical studies can provide some help in designing highly efficient phosphorescent materials.

Acknowledgment. This work was supported by the Natural Science Foundation of China (Grant Nos. 20173021, 20333050, and 20573042).

Supporting Information Available: Tables S1−S4, giving orbital compositions of complexes **2** and **3** in the ground and excited states and a table of Cartesian coordinates of optimized structures for **1**−**4**. This material is available free of charge via the Internet at http://pubs.acs.org.

OM0606338